Article

Effective Entanglement and Constraint Release in Deformed Polymer Melts

Lin-Feng Wu, Long-Fei Mao, and Zhe Wang*

Read Online

ACCESS | Metrics & More | Article Recommendations | Supporting Information

ABSTRACT: Quantifying the response of entangled polymers to large and rapid deformations presents a great challenge in polymer physics. With simulation results, we identify the effective entanglement that governs the chain conformation and rheological response of deformed entangled polymers. The distribution of effective entanglements gives a natural estimation of the mean survival tube. The constraint release caused by the motion of effective entanglements well describes the relaxation process after step elongation within the framework of the tube model. The relation between the dynamics of effective entanglements and other motions, including the orientation, stretch, and retraction of chain segments, is examined. Additionally, with small-angle neutron scattering, we experimentally explored the effective entanglements during the relaxation of an elongated polystyrene melt. We observe a "Rouse ramp" in the decay of effective entanglements, which is considered a key feature of the tube relaxation induced by the constraint release.
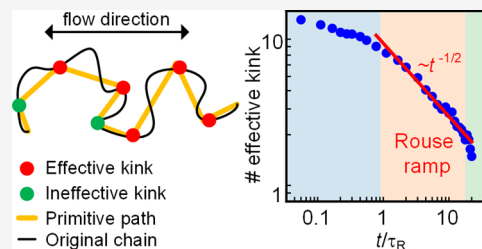
I. INTRODUCTION

Our current understanding of polymer dynamics is primarily built on the tube concept,[1] which models the constraints on the chain motion imposed by interchain entanglements as a mean-field, smooth tube along its own primitive path (PP). With several key relaxation mechanisms including reptation,[2] contour length fluctuation (CLF),[3] and constraint release (CR),[4−6] the tube model has been remarkably successful in describing the linear rheology of entangled polymers.[7] However, the modeling for the responses to large and rapid deformations is still challenging.[8,9] For example, the generalized tube model,[10] which incorporates convective constraint release[11,12] and chain stretch and retraction,[13] fails in predicting the nonlinear rheology in the extensional flow.[14−16] Particularly, the roles of chain conformations,[17,18] entanglement behaviors,[19−22] and dissipative properties[14,23] in determining the nonlinear rheology remain in debate.

To tackle these problems, clarifying the microscopic foundation of entanglement in strongly deformed polymers is of great importance. Experimental probes, such as small-angle neutron scattering (SANS)[24−26] and neutron spin echo (NSE),[27] have not provided direct observations of entanglements and their evolution. Molecular dynamics (MD) simulations, on the other hand, have shed significant light on this problem. Based on the pioneering contribution from Kremer and Grest,[28] PPs are identified either by fixing chain ends and imposing chain shrinkage[29−34] or by finding the average position of monomers.[35−39] Then, entanglements are located as contacts between PPs. The dynamics of entanglement in flow has also been subject to simulation investigation, revealing the influence of strain rate on the system.[40−42] Nevertheless, most of these studies do not show a systematic

comparison among the tube model prediction, the mechanical response, and the CR effect deduced from their microscopic definitions of entanglements in the nonlinear regime. Further clarifying the microscopic picture of entanglements, the associated CR process, and their coupling to other motions such as the orientation, stretch, and retraction of chain segments is important for improving the constitutive modeling of the nonlinear rheology of polymers.

In the tube model, the entanglements confining transverse motions of a test chain are abstracted as a continuous tube to deal with single-chain dynamics, e.g., reptation, chain retraction, and CLF. For the CR motion, occurring when the end of a neighboring chain passes the test chain, a detailed, discrete viewpoint on entanglements is needed to understand its dynamics and rheological consequences, which makes its experimental validation at the molecular level more difficult. Most previous experimental studies investigate the CR effect at the macroscopic level through rheological means.[8] At the molecular level, NSE result has shown the necessity of introducing the CR mechanism into the tube model in explaining the short-time dynamics of binary systems.[27] However, due to the dynamic limit of NSE, the effect of CR in the whole dynamic regime of the relaxation of the test chain
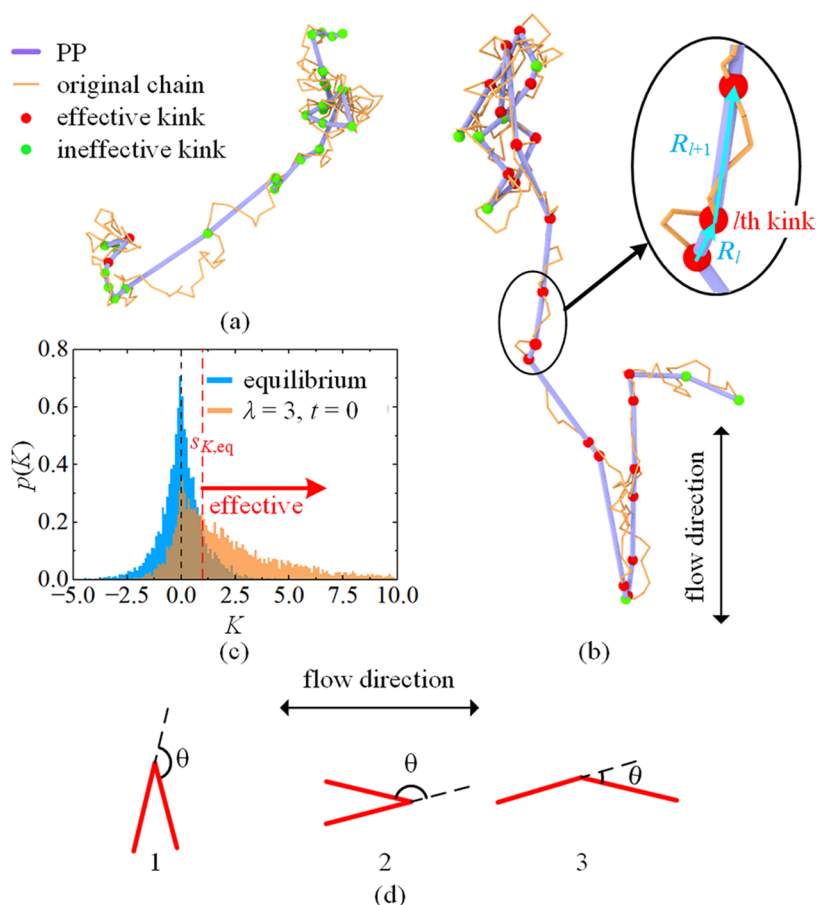
Figure 1. PPs of a chain with $N = 1000$ before (a) and immediately after (b) elongation to $\lambda = 3$ (thick lines). The effective and ineffective kinks are denoted by red and green symbols, respectively. The original chains are presented by thin lines. (c) Probability distributions of K of the melt with $N = 1000$ before and immediately after elongation to $\lambda = 3$. (d) Comparison between the significant kink defined by Hsu and Kremer (nos. 1 and 2) and the effective entanglement defined in this work (nos. 2 and 3).

cannot be accessed. To further explore the CR motion experimentally, new insight into entanglements is in demand.

Herein, we investigate the entanglement and CR in deformed linear polymers by employing MD simulation and SANS. With MD results, we propose the effective entanglement that governs the chain conformation of deformed polymers. The statistical distribution of effective entanglements naturally gives the mean survival tube. The CR process arising from the dynamics of effective entanglements describes well the relaxation after a step elongation within the framework of the tube model. Moreover, we propose a model to extract effective entanglements from the SANS spectra of deformed polymers. With this model, we observe the "Rouse ramp"[8,43] in the relaxation of effective entanglements, which is considered as the major feature of CR but has not been observed microscopically before.

The rest of the article is organized as follows. In Section II, we identify the effective entanglement in deformed polymers from the MD data. The role it plays in the chain conformation and the nonlinear rheological response is discussed. Section III introduces a SANS model for experimentally extracting the effective entanglement. The result of the SANS experiment on a set of entangled polystyrene melts is given. Concluding remarks are listed in Section IV.

II. EFFECTIVE ENTANGLEMENT FROM MD

We simulate 3 melts of $M_c = 250$ bead–spring chains[28] of N beads with $N = 700$, 1000, and 1500 using LAMMPS.[44] All beads interact via the repulsive Lennard-Jones (LJ) potential, and the beads within the same chain are connected by the finite-extensible nonlinear elastic potential.[28] The units of energy, length, and time are, respectively, set by ϵ, σ, and $\tau = \sigma(m/\epsilon)^{1/2}$, where ϵ and σ are LJ parameters and m is the monomer mass. The melts are equilibrated at density $\rho = 0.85\sigma^{-3}$ and temperature $T = 1\epsilon/k_B$, where k_B is the Boltzmann factor. For this condition, the equilibrium number of monomers per entanglement N_e and the Rouse time of an entangled strand τ_e are set to $N_e = 60$ and $\tau_e = 3290\tau$ as suggested by Cao and Likhtman.[45] Melts are strained by isochoric elongation along the z axis to the desired stretch ratio λ ranging from 1.8 to 5 at an initial Rouse Weissenberg number $Wi_{R,i} = \tau_R\dot{\epsilon}_i = 40$, where $\tau_R = (N/N_e)^2\tau_e$ is the Rouse time of the chain and $\dot{\epsilon}_i$ is the initial strain rate. During the elongation, the engineering strain rate keeps constant.

II.I. Effective Entanglement in Deformed Polymers. We use Z1+ code[46] to identify PPs and kinks as the contacts between PPs. Z1+ code monotonically reduces the contour length of chain while maintaining the noncrossing constraint between chains, under the condition of fixed chain ends. The resulting PP is composed of many straight strands, and PP length L is obtained by summing the lengths of these strands.

Figure 1a,b gives the PPs of a chain with $N = 1000$ before and immediately after elongation to $\lambda = 3$, respectively. The kinks, separating a PP into successively connected straight strands, can be considered as candidates for entanglements. In an elongated chain, the entropic tensile stress σ_t depends on the alignment of strands arising from orientation or stretch by $\sigma_t = \sigma_{zz} - \sigma_{xx} \sim \sum_l (R_{l,z}^2 - R_{l,x}^2)/N_{s,l}$, where $R_{l,z/x}$ is the z/x component of the end-to-end vector $\mathbf{R}_l$ of the lth strand and $N_{s,l}$ is the number of monomers contained in the lth strand. Thus, we can evaluate the alignment of tube segments around the lth kink by the following quantity:

$$K = \frac{R_{l,z}^2 - R_{l,x}^2}{N_{s,l}} + \frac{R_{l+1,z}^2 - R_{l+1,x}^2}{N_{s,l+1}} \quad (1)$$

where the subscripts "l" and "$l + 1$" denote the two strands that are connected at the lth kink. Figure 1c shows the distributions of K of the melt with $N = 1000$ before and after elongation. We use the standard deviation $s_{K,\text{eq}}$ of the equilibrium distribution of K as a threshold and pick out the kinks with $K > s_{K,\text{eq}}$ in the strained melt as the effective entanglements, in the sense that the local tube segments around these kinks are significantly aligned to the flow direction and contribute to stress. The effective kinks are denoted in Figure 1a,b. One may be interested in the difference between the effective kink defined here and the significant kink proposed by Hsu and Kremer.[21,22] Using the primitive path analysis,[29] Hsu and Kremer investigate the kinks in strongly deformed melts and pick out those with sharp bond angle θ, typically $\theta \geq 60°$, as the ones important for mechanical responses. Figure 1d-1,d-2 gives two examples of the significant kink. According to our definition of effective entanglement, the kinks shown in Figure 1d-2,d-3 are effective because their adjacent strands are highly aligned to the flow direction. In strongly elongated melts, effective kinks can be more prevalent due to the orientation and stretch of chains along the flow direction.

Note that the unstrained melt also contains a few effective kinks. Thus, as to the mean number of effective entanglements per chain Z_{ee}, we subtract such background to reduce the random thermal effect:

$$Z_{\text{ee}} = (n_{\text{ee,def}} - n_{\text{ee,eq}})/M_c \quad (2)$$

where $n_{\text{ee,eq}}$ and $n_{\text{ee,def}}$ are the average numbers of effective entanglements in the melt before and after deformation, respectively.

We will put emphasis on the relaxation dynamics after a strong step strain, which plays a crucial role in understanding the nonlinear rheology.[1] Figure 2a shows the relaxation of the tensile stress σ_t of the melt with $N = 1000$ after elongation to $\lambda = 3$ calculated by $\sigma_{\alpha\beta} = -\langle \sum_{ij} f_{ij,\alpha} r_{ij,\beta} \rangle/2V$, where the sum is over all pairs of beads, and f, r, and V denote force, separation, and volume, respectively. In the tube model, the relaxation at $t > \tau_e$ is composed of fast chain retraction, reptation, and CR motion:[1,6]

$$\frac{\sigma_t(t)}{\sigma_t(0)} = \left[\frac{L(t)}{L(0)}\right]^2 \psi(t) R(t) \quad (3)$$

where $\psi(t)$ is the fraction of PP that has not escaped from the original tube after a time t deduced from single-chain effects, $L(t)$ denotes the PP length at time t, and $R(t)$ represents the CR effect. $\psi(t)$ is given by $\psi(t) = \sum_{p:\text{odd}}(8/p^2\pi^2)\exp(-p^2 t/\tau_d)$, where τ_d is the chain disengagement time.[1] As to $L(t)$, recent
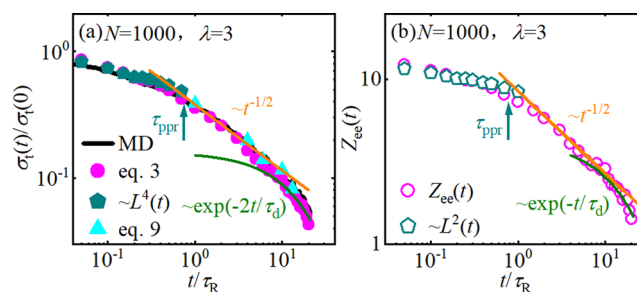
Figure 2. (a) Stress relaxation of the melt with $N = 1000$ and $\lambda = 3$. Black solid lines denote the MD result found by $\sigma_{\alpha\beta} = -\langle \sum_{ij} f_{ij,\alpha} r_{ij,\beta} \rangle/2V$. Magenta circles and cyan triangles denote the results found with eqs 3 and 9, respectively. (b) Decay of Z_{ee} of the melt with $N = 1000$ and $\lambda = 3$ (open circles).

studies show that its retraction cannot be described by a simple exponential form.[47,48] We find that it can be fitted by the form of stretched exponential decay:

$$\frac{L(t)}{L_{\text{eq}}} = 1 + \left[\frac{L(0)}{L_{\text{eq}}} - 1\right]\exp\left[-\left(\frac{t}{\tau_{\text{ppr}}}\right)^\beta\right] \quad (4)$$

where L_{eq} is the equilibrium PP length, τ_{ppr} is the characteristic time of PP retraction, and β is the stretching exponent ($\beta < 1$).[49] Figure 3 shows the evolution of $L(t)$ of the melt with $N =$
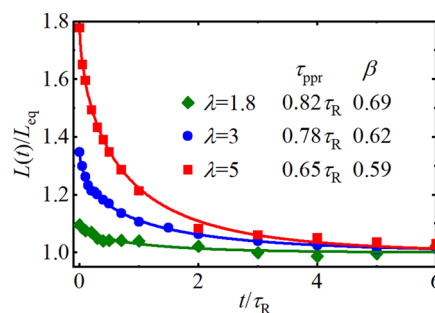
Figure 3. Retraction of the PP length $L(t)$ of the $N = 1000$ melt at $\lambda = 1.8$, 3, and 5 (symbols). Solid lines denote the fits with the stretched exponential decay form eq 4. The fitting parameters are presented in the figure.

1000 after elongation to $\lambda = 1.8$, 3, and 5, and curves fitted with eq 4. The emergence of the less-than-one stretching exponent β could be due to the heterogeneous dynamics of chain relaxation.[48,49] It is seen that the value of τ_{ppr} decreases as the chain stretch enhances. This observation is consistent with a recent simulation study,[18] which suggests that stronger chain stretch stimulates faster modes with shorter wavelengths, consequently resulting in faster chain retraction.

For a deformed chain, the release of an effective entanglement leads to relaxation of the local orientation and stress. Therefore, $R(t)$ can be tentatively represented by the decay of $Z_{\text{ee}}(t)$. Figure 2b shows the case of $Z_{\text{ee}}(t)$. At $t < \tau_{\text{ppr}}$, the fast decrease of Z_{ee} should be mainly due to the PP retraction,[10] which implies $Z_{\text{ee}}(t) \sim L^2(t)$. This is indeed the case for the results shown in Figure 2a,b, while it does not work for $\lambda = 1.8$ due to the weak chain stretch/retraction[50] and the major mechanism here could be the CLF.[27] As seen from Figure 3, the value of $[L(0)/L_{\text{eq}}]^2$ at $\lambda = 1.8$ is only 1.20. For comparison, those at $\lambda = 3$ and 5 are 1.81 and 3.16,
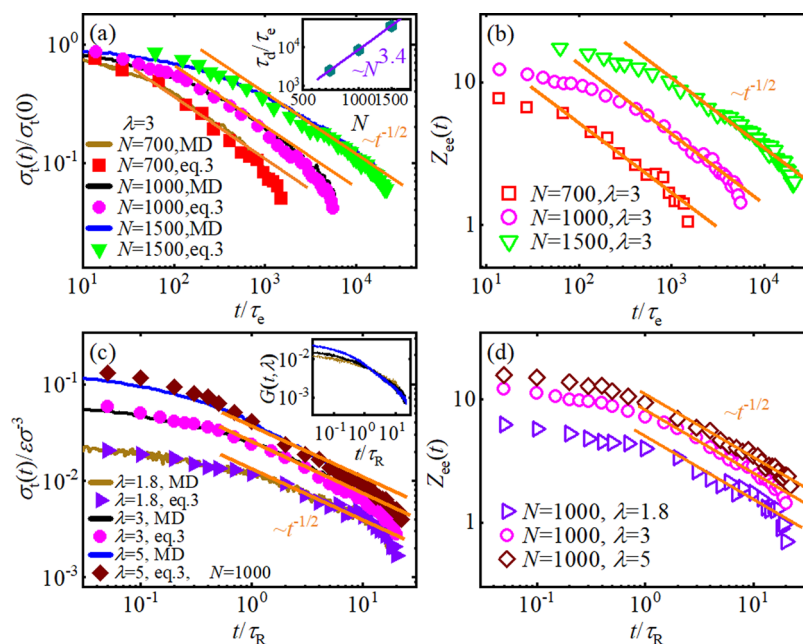
Figure 4. Stress relaxation (a) and decay of Z_{ee} (b) for $N = 700$, 1000, and 1500 at $\lambda = 3$. The inset in (a) shows the N dependence of τ_d. Stress relaxation (c) and decay of Z_{ee} (d) of the melt with $N = 1000$ at $\lambda = 1.8$, 3, and 5. The inset in (c) shows the superposition of the stress relaxation curves, $G(t,\lambda) = \sigma_t(t)/h_{RP}(\lambda)$. In all panels, we denote the $t^{-1/2}$ law by orange solid lines.
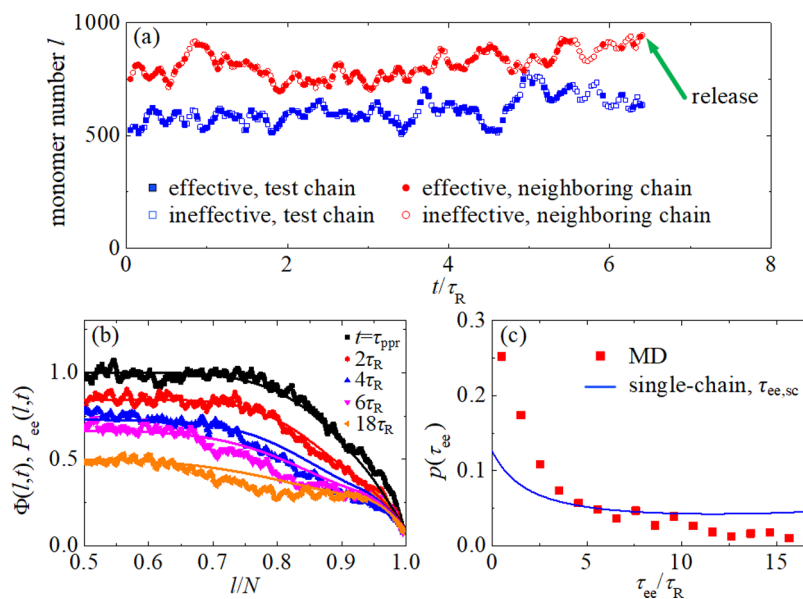
Figure 5. Entanglement dynamics of the melt with $N = 1000$ and $\lambda = 3$. (a) Monomers participating in a kink that is effective at $t = 0$ as a function of time. Solid and open symbols denote the effective and ineffective states, respectively. (b) Evolutions of the distribution of effective entanglements along PP $P_{ee}(l,t)$ (symbols) and segment survival probability $\Phi(l,t)$ (lines) at $t \geq \tau_{ppr}$. The data of $P_{ee}(l,t)$ are multiplied by a numerical factor to compare with those of $\Phi(l,t)$. In calculating $\Phi(l,t)$, we correct for the dangling-end effect. (c) Distribution of the lifetime τ_{ee} of the entanglements that are effective at $t = 0$ (symbols). The distribution calculated by only considering single-chain mechanisms is denoted by the solid line for comparison.

respectively. Starting from $t \approx \tau_{ppr}$, $Z_{ee}(t)$ behaves as $t^{-1/2}$. This time dependence is the signature of the CR-induced Rouse-like tube relaxation, also known as the CR-Rouse motion.[8,43] At $t > 10\tau_R$, $Z_{ee}(t)$ decays exponentially with a characteristic time τ_{CR} due to the reptation of neighboring chains.[51,52] Representing $R(t)$ by the decay of effective entanglements, and setting τ_d in $\psi(t)$ to τ_{CR} as suggested by the double reptation picture,[51] we calculate $\sigma_t(t)$ using eq 3 and show the result in Figure 2a. It is seen that the tube model nicely describes stress relaxation.

Note that $\sigma_t(t)$ relaxes as $t^{-1/2}$ in the intermediate time range. This phenomenon, known as the "Rouse ramp", is a key prediction of the CR-Rouse model.[8,43] Similar phenomena were seen in previous simulation[18] and experimental[53,54] data of stress relaxation (some previous data are summarized in the Appendix), while the microscopic origin has not been investigated in detail in these studies. Our analysis clearly shows that the CR-Rouse motion is governed by the dynamics of effective entanglements in deformed melts.

Above analysis suggests $\sigma_t(t) \sim \psi(t)Z_{ee}(t)$ at $t > \tau_{ppr}$. For this decoupling form, we discuss the following two points. (i) For entanglements adjacent to the ends of the test chain, they can be released through single-chain motions or CR. Thus, such decoupling form should be considered as an approximation for the well-entangled system in which the entanglements are plentiful. (ii) Considering that the Z_{ee} effective entanglements separate the test chain into $Z_{ee} + 1$ oriented strands, one may expect that $R(t) \propto Z_{ee}(t) + 1$. Additionally, the release of the last effective entanglement will give rise to the relaxation of the last two oriented strands. With these thoughts, the form of $R(t)$ can be written as $R(t) \propto Z_{ee}(t) + \exp(-t/\tau_d)$, in which $R(t)$ crosses over from $Z_{ee}(t) + 1$ to $Z_{ee}(t)$ at the terminal regime. Despite the above 2 points, we emphasize that the key role of effective entanglements in determining the chain conformation and the rheological response still holds.

We apply the same analysis to melts with different N and λ. Figure 4a,b compares the relaxations of melts with $N = 700$, 1000, and 1500 at $\lambda = 3$. The inset of Figure 4a gives τ_d as a function of N. τ_d grows with N as $N^{3.4}$. The exponent here agrees with the experimental value and is higher than the prediction of the reptation theory (3). This deviation was ascribed to the CLF.[3,7] Thus, we suggest that the τ_d found here reflects the single-chain mechanism, including both reptation and CLF. Figure 4c,d shows the relaxations of the $N = 1000$ melt at $\lambda = 1.8$, 3, and 5. According to the tube model, the stress relaxations in these 3 cases are expected to exhibit time-strain separability.[1] To test this property, we employ several common damping functions to superpose the stress relaxation data: the classical network stress−strain relation $h(\lambda) = \lambda^2 - \lambda^{-1}$, the Doi−Edwards damping function,[1] and the Rubinstein−Panyukov damping function $h_{RP}(\lambda) = (\lambda^2 - \lambda^{-1})/(\lambda - \lambda^{0.5} + 1)$.[55] It turns out that the Rubinstein−Panyukov function gives the best superposition, as shown in the inset of Figure 4c. For the sake of consistency, we use the average stretch ratio of chains $\bar{\lambda}_c$, rather than the stretch ratio of melt λ, to calculate the damping function. Here, the values of $\bar{\lambda}_c$ are 1.76, 2.82, and 4.52, slightly smaller than those of λ. In fact, both λ and $\bar{\lambda}_c$ well superimpose the stress data with $h_{RP}(\lambda)$. This damping function is derived based on the strain-dependent nonaffinity of the monomer distribution. We will get back to this point in our SANS model in Section III. In all relaxations shown in Figure 4a−d, the Rouse ramp is present.

II.II. Dynamics of Effective Entanglement. We trace the time evolution of all effective entanglements that exist at the beginning of the relaxation ($t = 0$) of the melt with $N = 1000$ stretched to $\lambda = 3$. We perform the PP analysis every $0.3\tau_e$ and mark the monomers participating in each kink. Figure 5a shows the monomers participating in a kink that is effective at $t = 0$ as a function of time. It is seen that this kink is not always effective or even disappears sometimes due to the rapid fluctuation of chains.[36] Previous studies employ time and iso-configurational ensemble averaging[38] to reduce such thermal fluctuation. This procedure, though useful in obtaining a smooth PP, makes the simulation and data analysis computation-consuming. In fact, the pivotal dynamical quantity for justifying the tube model is the segment survival probability of the mean tube rather than the tube of a specific chain. We can estimate the survival part of the mean tube with the statistical distribution of effective entanglements along PP without time or iso-configurational averaging. Figure 5b shows the evolution of the distribution of effective entanglements

along PP $P_{ee}(l,t)$ as a function of monomer number l at $t \geq \tau_{ppr}$, during which the PP almost retracts to its equilibrium length. According to the tube picture, for $t \geq \tau_{ppr}$, the segment survival probability $\Phi(l,t)$, i.e., the probability that the segment containing monomer l is still in the original tube at time t, is proportional to $\psi(l,t)Z_{ee}(t)$, where $\psi(l,t) = \sum_{p:odd}(4/p\pi)\sin(p\pi l/N)\exp(-p^2t/\tau_d)$ is the equilibrium segment survival probability deduced from single-chain effects.[1] Figure 5b compares $P_{ee}(l,t)$ and $\Phi(l,t) \sim \psi(l,t)Z_{ee}(t)$, and a nice agreement is seen. This result suggests that the distribution of effective entanglements can be considered as an indicator of the survival tube for deformed polymers.

We identify the destruction of a kink by one chain's end passing the other chain, as denoted by the green arrow in Figure 5a. Figure 5c shows the distribution of the lifetime τ_{ee} values of the entanglements that are effective at the beginning of relaxation. Nearly half of these entanglements release within $t < \tau_{ppr}$ due to the PP retraction. For $t > \tau_{ppr}$, we also calculate the lifetime distribution considering only the single-chain effects. For an entanglement located at monomer l of the test chain, the expectation of its single-chain lifetime $\tau_{ee,sc}$ can be evaluated by $\psi(l,\tau_{ee,sc}) = e^{-1}$. As seen from Figure 5c, the lifetime exhibits a significant propensity toward higher values if only the single-chain effect is considered. This result highlights the influence of CR on the dynamics of entanglements.

III. EFFECTIVE ENTANGLEMENT FROM SANS

We explore effective entanglements experimentally in this section. SANS can measure the single-chain form factor $S(Q)$ (Q is the scattering vector of neutron) of polymer melts with the aid of deuterium labeling.[24] For equilibrium melts, however, $S(Q)$ is not affected by entanglements and is well described by the Debye function,[26] making the probing of entanglements impossible. For deformed melts, on the other hand, entanglements induce deformation-dependent non-affinity at length scales comparable to the PP step,[55−57] suggesting that one can quantify the distribution of entanglements by characterizing such nonaffinity. By modeling tube confinement with virtual chains acting on the test chain, Rubinstein and Panyukov propose an affine monomer separation $N_{aff} = \lambda N_e$,[55] in the sense that for monomers i and j in a deformed chain, their displacement undergoes affine deformation if $|i - j| > N_{aff}$, while nonaffinity emerges at $|i - j| < N_{aff}$. Notice that N_{aff} is also the separation between two adjacent virtual "cross-links" that connect to virtual chains. Figure 6a illustrates the idea of this nonaffine tube model (NTM).

III.I. SANS Model. Inspired by NTM, we propose a model for the analysis of SANS spectra of deformed entangled melts. It is seen that the effective entanglements play a critical role in confining the deformed chain. Thus, we assume that the length of the PP step of a deformed chain is determined by the separation between two adjacent effective entanglements N_{ee} ($N_{ee} = N/(Z_{ee} + 1)$), while the ineffective kinks and relaxed neighboring chains give no orientational constraint. This is somewhat similar to the "tube dilation" picture,[58,59] which assumes that the PP step (or tube diameter) is determined by unrelaxed strands and, consequently, increases with time due to the release of the initial entanglements. Then, borrowing the idea of NTM, we obtain the affine monomer separation as $N_{aff} = \lambda N_{ee}$. To avoid the unphysical situation of $N_{aff} > N$ at large λ, we practically correct N_{aff} as
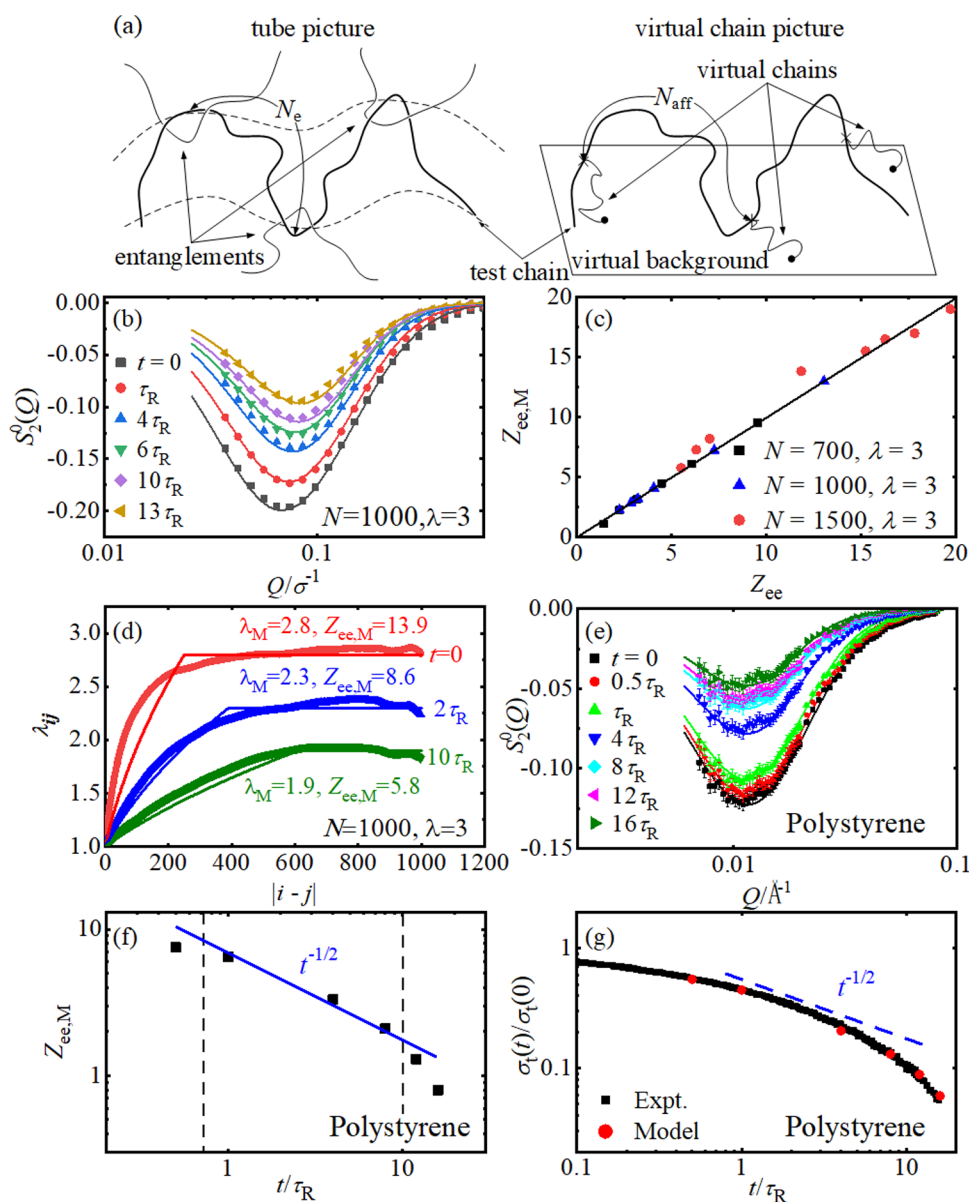
Figure 6. Nonaffine tube model (NTM) analysis. (a) Illustration of the NTM. (b) $S_2^0(Q)$ in the relaxation of the melt with $N = 1000$ and $\lambda = 3$ (symbols) and model-fitting curves (lines). (c) Scatter plot of the number of effective entanglements per chain found from NTM analysis $Z_{ee,M}$ and that from eq 2 with Z1 + code Z_{ee}. (d) Separation-dependent stretch ratio λ_{ij} as a function of monomer separation $|i − j|$ in the relaxation of the melt with $N = 1000$ and $\lambda = 3$ at $t = 0$, $2\tau_R$, and $10\tau_R$ (symbols). Results calculated with NTM parameters λ_M and $Z_{ee,M}$ are also shown (lines). (e) $S_2^0(Q)$ in the relaxation of the polystyrene melt after a step elongation to $\lambda = 1.8$ (symbols) and the model-fitting curves (lines). (f) Decay of $Z_{ee,M}$ of the polystyrene melt. (g) Stress relaxation of the polystyrene melt (black squares). The results calculated by the NTM parameters are also given (red circles).

$$N_{aff} = N\left[1 - \exp\left(-\lambda\frac{N_{ee}}{N}\right)\right] = N\left[1 - \exp\left(-\frac{\lambda}{Z_{ee} + 1}\right)\right] \tag{5}$$

For $|i − j| > N_{aff}$, the probability $\phi(i,j,\boldsymbol{r})$ of finding monomer j at distance $\boldsymbol{r}$ from monomer i is given by an affine Gaussian form:

$$\phi(i, j, \boldsymbol{r}) = \left(\frac{3}{2\pi|i − j|b^2}\right)^{3/2}$$
$$\times \exp\left[-\frac{3}{2|i − j|b^2}\left(\lambda_M r_x^2 + \lambda_M r_y^2 + \frac{r_z^2}{\lambda_M^2}\right)\right],$$
$$|i − j| \geq N_{aff} = N[1 - e^{-\lambda_M/(Z_{ee,M}+1)}] \tag{6}$$

where b is the bond length and the subscript "M" denotes model parameters. For $|i − j| < N_{aff}$, monomers i and j are within a strand between two adjacent virtual cross-links. Their distribution depends on the end-to-end vector of this strand $\boldsymbol{R}_s$. This conditional probability $\phi(i,j,\boldsymbol{r}|\boldsymbol{R}_s)$ is simply approximated by a bivariate Gaussian form.[60,61] Then, $\phi(i,j,\boldsymbol{r})$ is found as[57,60]

$$\phi(i, j, \boldsymbol{r}) = \left(\frac{\beta^2}{\pi w_{ij}}\right)^{3/2}$$

$$\times \sqrt{\frac{1}{(w_{ij}/\lambda_{\mathrm{M}} + 1 - w_{ij})^2 (w_{ij}\lambda_{\mathrm{M}}^2 + 1 - w_{ij})}}$$

$$\times \exp\left[-\frac{\beta^2}{w_{ij}}\left(\frac{r_x^2 + r_y^2}{w_{ij}/\lambda_{\mathrm{M}} + 1 - w_{ij}}\right.\right.$$

$$\left.\left. + \frac{r_z^2}{w_{ij}\lambda_{\mathrm{M}}^2 + 1 - w_{ij}}\right)\right],$$

$$|i - j| < N_{\mathrm{aff}} = N[1 - e^{-\lambda_{\mathrm{M}}/(Z_{\mathrm{ee,M}}+1)}] \qquad (7)$$

where $\beta^2 = 3/2N_{\mathrm{aff}}b^2$ and $w_{ij} = |i - j|/N_{\mathrm{aff}}$. Knowing $\phi(i,j,\boldsymbol{r})$, $S(\boldsymbol{Q})$ can be calculated through the method given in our previous paper.[57] The details of the model, the calculation of $S(\boldsymbol{Q})$, and the following analyses are given in the Supporting Information. In this model, the chain conformation is characterized by two model parameters: the stretch ratio λ_{M} and the number of effective entanglements per chain $Z_{\mathrm{ee,M}}$. The relaxation of a deformed chain is reflected by decreasing λ_{M} and $Z_{\mathrm{ee,M}}$. This picture, assuming uniform relaxation of orientation and effective entanglement density along the PP, is oversimplified. Its usability must be tested by MD results.

As we demonstrate in ref[62], the anisotropy of extensional chains can be quantified by expanding $S(\boldsymbol{Q})$ in spherical harmonics as $S(\boldsymbol{Q}) = \sum_{l:even} S_l^0(Q) Y_l^0(\hat{\boldsymbol{Q}})$, and the coefficient $S_2^0(Q)$ reflects the main anisotropic feature. Figure 6b shows the $S_2^0(Q)$ in the relaxation of the melt with $N = 1000$ and $\lambda = 3$ and the model-fitting curves. By fitting $S_2^0(Q)$, λ_{M} and $Z_{\mathrm{ee,M}}$ are obtained. Figure 6c displays good agreement between the fitted $Z_{\mathrm{ee,M}}$ and the Z_{ee} found with the Z1+ code. In Figure 6d, we show the evolution of separation-dependent stretch ratio λ_{ij} as a function of monomer separation $|i - j|$. λ_{ij} is calculated by

$$\lambda_{ij} = \sqrt{\langle \overline{R_z^2 (|i - j|)} \rangle} / \sqrt{\langle \overline{R_z^2 (|i - j|)} \rangle_{\mathrm{eq}}} \qquad (8)$$

where $R_z(|i - j|)$ is the flow direction component of the end-to-end vector of the strand from monomer i to monomer j, the overline denotes the average over monomers on a test chain, $\langle \cdots \rangle$ denotes the average over all chains, and the subscript "eq" denotes that the calculation is performed at the equilibrium state. As seen from Figure 6d, as $|i - j|$ increases, λ_{ij} grows to a plateau at $|i - j| \approx N_{\mathrm{aff}}$, and it slightly decreases as $|i - j|$ approaches N due to faster relaxation at the two chain ends and the dangling-end effect. The λ_{ij} values calculated from the NTM with fitted λ_{M} and $Z_{\mathrm{ee,M}}$ are also shown. λ_{M} is seen to nicely evaluate the plateau of λ_{ij}. Moreover, the increase in nonaffinity during the relaxation is captured by the decay of $Z_{\mathrm{ee,M}}$. The tensile stress in the NTM is given by[55]

$$\sigma_{\mathrm{t,M}} = \frac{M_{\mathrm{c}}}{V} kT (Z_{\mathrm{ee,M}} + 1)(\lambda_{\mathrm{M}} - \lambda_{\mathrm{M}}^{-1} + \lambda_{\mathrm{M}}^{1/2} - \lambda_{\mathrm{M}}^{-1/2})$$

$$(9)$$

The decay of $\sigma_{\mathrm{t,M}}$, shown in Figure 2a, matches the stress relaxation. Assuming that the chain is formed by strands connected by virtual cross-links, one may use the stress expression for network, expressed as $\sigma_{\mathrm{t,M}} = M_{\mathrm{c}}kT(Z_{\mathrm{ee,M}} + 1)(\lambda_{\mathrm{M}} - \lambda_{\mathrm{M}}^{-2})/V$,[63] to replace eq 9. These two equations give very similar results for the decay of normalized stress in our cases.

III.II. SANS Result. After verifying the effectiveness of the NTM in extracting Z_{ee} and chain conformation, we reanalyze the SANS data from a set of highly monodisperse polystyrene melts that we have published in ref[57]. The samples are mixtures of protonated and deuterated polystyrene homopolymers with a d/h ratio of 10/90 (h-PS: $m_{\mathrm{w}} = 197$ kg/mol, $m_{\mathrm{w}}/m_{\mathrm{n}} = 1.01$; d-PS: $m_{\mathrm{w}} = 213$ kg/mol, $m_{\mathrm{w}}/m_{\mathrm{n}} = 1.06$, and m_{w} and m_{n} are weight-average and number-average molecular weights, respectively). According to ref[64], the equilibrium number of entanglements per chain Z_{eq} of the sample is 13.8. The isotropic samples were uniaxially stretched to $\lambda = 1.8$ at 124 °C with a constant crosshead velocity $v = 8l_0/\tau_{\mathrm{R}}$, where l_0 is the initial length of the sample. The stretched samples were allowed to relax for different amounts of time at 124 °C at constant strain and then immediately quenched to the glassy state for the *ex situ* SANS measurement. More details about samples and the SANS experiment are given in the Supporting Information.

Figure 6e shows the $S_2^0(Q)$ of the sample immediately after the stretch to $\lambda = 1.8$ and those during the subsequent relaxation. The fitted curves are also shown. Figure 6f shows the decay of $Z_{\mathrm{ee,M}}$. Right after the stretch, $Z_{\mathrm{ee,M}}$ is 11.8, close to Z_{eq}. At $t > \tau_{\mathrm{R}}$, a Rouse ramp is seen, which provides direct microscopic evidence for the Rouse-like tube relaxation induced by the CR of effective entanglements. Considering that the polystyrene sample and the simulated melt with $N = 1000$ and $\lambda = 1.8$ have comparable flow condition and entanglement number, we compare their relaxation processes in Figure S6 in the Supporting Information. Both the evolution of effective entanglements and the decay of $S_2^0(Q)$ exhibit similar behaviors for these two systems, suggesting that our simulation and data analysis capture the major physical characteristics of entangled melts.

Figure 6g shows the tensile stress relaxation of the polystyrene measured by a rheometer and that calculated with the NTM fitting and eq 9. Again, the calculated stress well captures the stress relaxation. The stress relaxation in this case does not exhibit a sharp $t^{-1/2}$ decay. The reason could be that the chain deformation is not large enough, which results in a strong coupling between the effects caused by CR and by single-chain motions. As λ or flow rate increases, the chain retraction becomes faster and stronger,[18] leading to a clearer separation between its effect and the subsequent CR process, and a sharp $t^{-1/2}$ decay can be found.[18,53] Interested readers are referred to the Appendix for more data and discussion about this point.

IV. CONCLUSIONS

In summary, we identify the effective entanglement in deformed polymers based on the PP analysis. The distribution of effective entanglements reflects the survival probability of the tube segments. The CR effect caused by the motion of effective entanglements results in a Rouse ramp in the intermediate range of relaxation, which fits well with the tube model complemented by the CR-Rouse effect. These results suggest the importance of effective entanglements in determining the conformation and rheological response of deformed polymers. By noticing the strain-dependent local nonaffinity, we propose a model to extract effective entanglements from SANS spectra. Applying it to the relaxation of an entangled polystyrene melt, a Rouse ramp is clearly revealed, providing experimental evidence of the CR-Rouse motion at the molecular level.

■ APPENDIX

In this study, we show that the stress relaxation exhibits a $t^{-1/2}$ power-law decay after the chain retraction and before entering the terminal regime. In fact, similar phenomena can be found in many previous simulation and experimental data. In Figure 7, we replot some data of stress relaxation after step elongation.
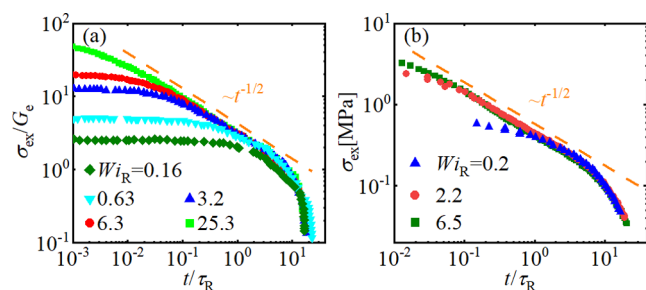
Figure 7. Data of stress relaxation after step elongation reproduced from refs 18 and 53. (a, b) Simulation and experimental data, respectively.

Figure 7a shows the simulation results of Kremer-Grest bead–spring polymer melts with $N = 500$ and Hencky strain $\varepsilon_H \approx 6$.[18] Figure 7b shows the experimental data of stress relaxation following steady extensional flow of a 285 kg/mol polystyrene melt at 130 °C.[53] The $t^{-1/2}$ decay is clearly seen in both panels. Moreover, it is seen that such feature emerges earlier and becomes more pronounced as the flow rate enhances.

The $t^{-1/2}$ law can also be found in the relaxation process after step shear. Figure 8 reproduces the relaxation data after
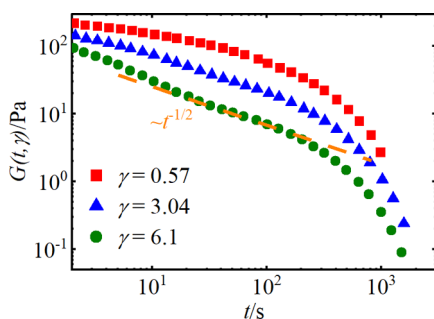
Figure 8. Data of relaxation modulus $G(t, \gamma)$ after step shear reproduced from ref 54.

step shear from ref 54. The sample is polystyrene solution of chlorinated biphenyl with a concentration of 0.06 g/cm^3 at 30 °C. The molecular weight of the polymer is 8.42×10^6. As seen from Figure 8, the $t^{-1/2}$ law emerges at the strain $\gamma = 3.04$ and becomes more prominent as γ increases. Note that, for cases shown in Figure 7, the strain is fixed while the flow rate changes. A faster flow rate effectively suppresses the relaxation during the elongation process and, consequently, results in a stronger chain stretch. Summarizing the results shown in Figures 7 and 8, we conclude that the $t^{-1/2}$ decay becomes more prominent as the chain stretch enhances. A reason for this observation could be that the stronger chain stretch will stimulate faster modes with shorter wavelengths, which leads to faster chain retraction.[18] Then, the separation between the first (chain retraction) and the second (CR-Rouse) stages of stress relaxation is sharper, enhancing the manifestation of the $t^{-1/2}$ law.

■ ASSOCIATED CONTENT

Ⓢ Supporting Information

The Supporting Information is available free of charge at https://pubs.acs.org/doi/10.1021/acs.macromol.4c00204.

> Details of MD simulation, experiment, SANS model, and data analysis (PDF)

■ AUTHOR INFORMATION

Corresponding Author

Zhe Wang − *Department of Engineering Physics and Key Laboratory of Particle and Radiation Imaging (Tsinghua University) of Ministry of Education, Tsinghua University, Beijing 100084, China;* ⓞ orcid.org/0000-0003-4103-0751; Email: zwang2017@mail.tsinghua.edu.cn

Authors

Lin-Feng Wu − *Department of Engineering Physics and Key Laboratory of Particle and Radiation Imaging (Tsinghua University) of Ministry of Education, Tsinghua University, Beijing 100084, China*

Long-Fei Mao − *Department of Engineering Physics and Key Laboratory of Particle and Radiation Imaging (Tsinghua University) of Ministry of Education, Tsinghua University, Beijing 100084, China*

Complete contact information is available at:
https://pubs.acs.org/10.1021/acs.macromol.4c00204

Notes

The authors declare no competing financial interest.

■ ACKNOWLEDGMENTS

■ REFERENCES

(1) Doi, M.; Edwards, S. F. *The Theory of Polymer Dynamics*; Clarendon: Oxford, England, 1986.

(2) De Gennes, P. G. Reptation of a Polymer Chain in the Presence of Fixed Obstacles. *J. Chem. Phys.* **1971**, 55, 572−579.

(3) Doi, M. Explanation for the 3.4 power law of viscosity of polymeric liquids on the basis of the tube model. *J. Polym. Sci., Polym. Lett. Ed.* **1981**, 19, 265−273.

(4) Daoud, M.; De Gennes, P. G. Some remarks on the dynamics of polymer melts. *J. Polym. Sci., Polym. Phys. Ed.* **1979**, 17, 1971−1981.

(5) Graessley, W. W. Entangled linear, branched and network polymer systems—Molecular theories. *Adv. Polym. Sci.* **1982**, 47, 67−117.

(6) Rubinstein, M.; Colby, R. H. Self-consistent theory of polydisperse entangled polymers: Linear viscoelasticity of binary blends. *J. Chem. Phys.* **1988**, 89, 5291−5306.

(7) Likhtman, A. E.; McLeish, T. C. B. Quantitative Theory for Linear Dynamics of Linear Entangled Polymers. *Macromolecules* **2002**, 35, 6332−6343.

(8) Dealy, J. M.; Read, D. J.; Larson, R. G. *Structure and Rheology of Molten Polymers: from Structure to Flow Behavior and Back Again*; Hanser: Cincinnati, 2018.

(9) Wang, S.-Q. *Nonlinear Polymer Rheology: Macroscopic Phenomenology and Molecular Foundation*; Wiley, 2017.

(10) Graham, R. S.; Likhtman, A. E.; McLeish, T. C. B.; Milner, S. T. Microscopic theory of linear, entangled polymer chains under rapid deformation including chain stretch and convective constraint release. *J. Rheol.* **2003**, *47*, 1171−1200.

(11) Marrucci, G. Dynamics of entanglements: A nonlinear model consistent with the Cox-Merz rule. *J. Non-Newtonian Fluid Mech.* **1996**, *62*, 279−289.

(12) Likhtman, A. E.; Milner, S. T.; McLeish, T. C. B. Microscopic Theory for the Fast Flow of Polymer Melts. *Phys. Rev. Lett.* **2000**, *85*, 4550−4553.

(13) Mead, D. W.; Larson, R. G.; Doi, M. A Molecular Theory for Fast Flows of Entangled Polymers. *Macromolecules* **1998**, *31*, 7895−7914.

(14) Matsumiya, Y.; Watanabe, H. Non-Universal Features in Uniaxially Extensional Rheology of Linear Polymer Melts and Concentrated Solutions: A Review. *Prog. Polym. Sci.* **2021**, *112*, No. 101325.

(15) Bach, A.; Almdal, K.; Rasmussen, H. K.; Hassager, O. Elongational Viscosity of Narrow Molar Mass Distribution Polystyrene. *Macromolecules* **2003**, *36*, 5174−5179.

(16) Huang, Q.; Alvarez, N. J.; Matsumiya, Y.; Rasmussen, H. K.; Watanabe, H.; Hassager, O. Extensional Rheology of Entangled Polystyrene Solutions Suggests Importance of Nematic Interactions. *ACS Macro Lett.* **2013**, *2*, 741−744.

(17) O'Connor, T. C.; Alvarez, N. J.; Robbins, M. O. Relating Chain Conformations to Extensional Stress in Entangled Polymer Melts. *Phys. Rev. Lett.* **2018**, *121*, No. 047801.

(18) O'Connor, T. C.; Hopkins, A.; Robbins, M. O. Stress Relaxation in Highly Oriented Melts of Entangled Polymers. *Macromolecules* **2019**, *52*, 8540−8550.

(19) Zheng, Y.; Tsige, M.; Wang, S. Q. Molecular Dynamics Simulation of Entangled Melts at High Rates: Identifying Entanglement Lockup Mechanism Leading to True Strain Hardening. *Macromol. Rapid Commun.* **2023**, *44*, No. 2200159.

(20) Ianniruberto, G.; Marrucci, G. Convective constraint release (CCR) revisited. *J. Rheol.* **2014**, *58*, 89−102.

(21) Hsu, H.-P.; Kremer, K. Primitive Path Analysis and Stress Distribution in Highly Strained Macromolecules. *ACS Macro Lett.* **2018**, *7*, 107−111.

(22) Hsu, H.-P.; Kremer, K. Clustering of Entanglement Points in Highly Strained Polymer Melts. *Macromolecules* **2019**, *52*, 6756−6772.

(23) López-Barrón, C. R.; Burghardt, W. R.; Kweon, M. S. Local and Global Stretching of Polymer Chains during Startup of Extensional Flow. *ACS Macro Lett.* **2020**, *9*, 26−31.

(24) Higgins, J. S.; Benoît, J. C. *Polymers and Neutron Scattering*; Clarendon: Oxford, England, 1994.

(25) Bent, J.; Hutchings, L. R.; Richards, R. W.; Gough, T.; Spares, R.; Coates, P. D.; Grillo, I.; Harlen, O. G.; Read, D. J.; Graham, R. S.; et al. Neutron-Mapping Polymer Flow: Scattering, Flow Visualization, and Molecular Theory. *Science* **2003**, *301*, 1691−1695.

(26) Likhtman, A. E. Single-Chain Slip-Link Model of Entangled Polymers: Simultaneous Description of Neutron Spin−Echo, Rheology, and Diffusion. *Macromolecules* **2005**, *38*, 6128−6139.

(27) Zamponi, M.; Wischnewski, A.; Monkenbusch, M.; Willner, L.; Richter, D.; Likhtman, A. E.; Kali, G.; Farago, B. Molecular Observation of Constraint Release in Polymer Melts. *Phys. Rev. Lett.* **2006**, *96*, No. 238302.

(28) Kremer, K.; Grest, G. S. Dynamics of entangled linear polymer melts: A molecular-dynamics simulation. *J. Chem. Phys.* **1990**, *92*, 5057−5086.

(29) Everaers, R.; Sukumaran, S. K.; Grest, G. S.; Svaneborg, C.; Sivasubramanian, A.; Kremer, K. Rheology and Microscopic Topology of Entangled Polymeric Liquids. *Science* **2004**, *303*, 823−826.

(30) Kröger, M. Shortest multiple disconnected path for the analysis of entanglements in two- and three-dimensional polymeric systems. *Comput. Phys. Commun.* **2005**, *168*, 209−232.

(31) Shanbhag, S.; Kröger, M. Primitive Path Networks Generated by Annealing and Geometrical Methods: Insights into Differences. *Macromolecules* **2007**, *40*, 2897−2903.

(32) Tzoumanekas, C.; Theodorou, D. N. Topological Analysis of Linear Polymer Melts: A Statistical Approach. *Macromolecules* **2006**, *39*, 4592−4604.

(33) Shanbhag, S.; Larson, R. G. Identification of Topological Constraints in Entangled Polymer Melts Using the Bond-Fluctuation Model. *Macromolecules* **2006**, *39*, 2413−2417.

(34) Stephanou, P. S.; Baig, C.; Tsolou, G.; Mavrantzas, V. G.; Kröger, M. Quantifying chain reptation in entangled polymer melts: Topological and dynamical mapping of atomistic simulation results onto the tube model. *J. Chem. Phys.* **2010**, *132*, No. 124904.

(35) Read, D. J.; Jagannathan, K.; Likhtman, A. E. Entangled Polymers: Constraint Release, Mean Paths, and Tube Bending Energy. *Macromolecules* **2008**, *41*, 6843−6853.

(36) Likhtman, A. E.; Ponmurugan, M. Microscopic Definition of Polymer Entanglements. *Macromolecules* **2014**, *47*, 1470−1481.

(37) Likhtman, A. E. The tube axis and entanglements in polymer melts. *Soft Matter* **2014**, *10*, 1895−1904.

(38) Bisbee, W.; Qin, J.; Milner, S. T. Finding the Tube with Isoconfigurational Averaging. *Macromolecules* **2011**, *44*, 8972−8980.

(39) Cao, J.; Qin, J.; Milner, S. T. Finding Entanglement Points in Simulated Polymer Melts. *Macromolecules* **2015**, *48*, 99−110.

(40) Baig, C.; Mavrantzas, V. G.; Kröger, M. Flow Effects on Melt Structure and Entanglement Network of Linear Polymers: Results from a Nonequilibrium Molecular Dynamics Simulation Study of a Polyethylene Melt in Steady Shear. *Macromolecules* **2010**, *43*, 6886−6902.

(41) Jeong, S.; Baig, C. Molecular process of stress relaxation for sheared polymer melts. *Polymer* **2020**, *202*, No. 122683.

(42) Moghadam, S.; Saha Dalal, I.; Larson, R. G. Unraveling Dynamics of Entangled Polymers in Strong Extensional Flows. *Macromolecules* **2019**, *52*, 1296−1307.

(43) Viovy, J. L.; Rubinstein, M.; Colby, R. H. Constraint release in polymer melts: tube reorganization versus tube dilation. *Macromolecules* **1991**, *24*, 3587−3596.

(44) Thompson, A. P.; Aktulga, H. M.; Berger, R.; Bolintineanu, D. S.; Brown, W. M.; Crozier, P. S.; In 'T Veld, P. J.; Kohlmeyer, A.; Moore, S. G.; Nguyen, T. D.; et al. LAMMPS - a flexible simulation tool for particle-based materials modeling at the atomic, meso, and continuum scales. *Comput. Phys. Commun.* **2022**, *271*, No. 108171.

(45) Cao, J.; Likhtman, A. E. Simulating Startup Shear of Entangled Polymer Melts. *ACS Macro Lett.* **2015**, *4*, 1376−1381.

(46) Kröger, M.; Dietz, J. D.; Hoy, R. S.; Luap, C. The Z1+ package: Shortest multiple disconnected path for the analysis of entanglements in macromolecular systems. *Comput. Phys. Commun.* **2023**, *283*, No. 108567.

(47) Ruan, Y.; Lu, Y.; An, L.; Wang, Z.-G. Nonlinear Rheological Behaviors in Polymer Melts after Step Shear. *Macromolecules* **2019**, *52*, 4103−4110.

(48) Zhou, Y.; Schroeder, C. M. Dynamically Heterogeneous Relaxation of Entangled Polymer Chains. *Phys. Rev. Lett.* **2018**, *120*, No. 267801.

(49) Ediger, M. D. Spatially Heterogeneous Dynamics in Supercooled Liquids. *Annu. Rev. Phys. Chem.* **2000**, *51*, 99−128.

(50) Borger, A. L.; Huang, Q.; Hassager, O.; Kirkensgaard, J. J. K.; Almdal, K.; Mortensen, K. Stretch and orientational mode decoupling in relaxation of highly stretched polymer melts. *Phys. Rev. Res.* **2020**, *2*, No. 043119.

(51) Cloizeaux, J. D. Double Reptation *vs.* Simple Reptation in Polymer Melts. *Europhys. Lett.* **1988**, *5*, 437−442.

(52) Hou, J.-X.; Svaneborg, C.; Everaers, R.; Grest, G. S. Stress Relaxation in Entangled Polymer Melts. *Phys. Rev. Lett.* **2010**, *105*, No. 068301.

(53) Huang, Q.; Rasmussen, H. K. Stress relaxation following uniaxial extension of polystyrene melt and oligomer dilutions. *J. Rheol.* **2016**, *60*, 465−471.

(54) Osaki, K.; Nishizawa, K.; Kurata, M. Material time constant characterizing the nonlinear viscoelasticity of entangled polymeric systems. *Macromolecules* **1982**, *15*, 1068−1071.

(55) Rubinstein, M.; Panyukov, S. Nonaffine Deformation and Elasticity of Polymer Networks. *Macromolecules* **1997**, *30*, 8036−8044.

(56) Pyckhout-Hintzen, W.; Botti, A.; Heinrich, M.; Westermann, S.; Richter, D.; Straube, E. The length-scale dependence of strain in networks by SANS. *Appl. Phys. A: Mater. Sci. Process.* **2002**, *74*, s368−s370.

(57) Wang, Z.-Y.; Kong, D.; Yang, L.; Ma, H.; Su, F.; Ito, K.; Liu, Y.; Wang, X.; Wang, Z. Analysis of Small-Angle Neutron Scattering Spectra from Deformed Polymers with the Spherical Harmonic Expansion Method and a Network Model. *Macromolecules* **2018**, *51*, 9011−9018.

(58) Marrucci, G. Relaxation by reptation and tube enlargement: A model for polydisperse polymers. *J. Polym. Sci., Polym. Phys. Ed.* **1985**, *23*, 159−177.

(59) Watanabe, H.; Ishida, S.; Matsumiya, Y.; Inoue, T. Test of Full and Partial Tube Dilation Pictures in Entangled Blends of Linear Polyisoprenes. *Macromolecules* **2004**, *37*, 6619−6631.

(60) Ullman, R. Small angle neutron scattering from polymer networks. *J. Chem. Phys.* **1979**, *71*, 436−449.

(61) The bivariate Gaussian form assumes that the strand between two adjacent virtual cross-links is Gaussian. This is not always true if such strand undergoes very large strain or contains very few monomers, where the distribution of monomers within the strand is no longer Gaussian-like.

(62) Wang, Z.; Lam, C. N.; Chen, W.-R.; Wang, W.; Liu, J.; Liu, Y.; Porcar, L.; Stanley, C. B.; Zhao, Z.; Hong, K.; Wang, Y. Fingerprinting Molecular Relaxation in Deformed Polymers. *Phys. Rev. X* **2017**, *7*, No. 031003.

(63) Rubinstein, M.; Colby, R. H. *Polymer Physics*; Oxford University Press, 2003.

(64) Fetters, L. J.; Lohse, D. J.; Richter, D.; Witten, T. A.; Zirkel, A. Connection between Polymer Molecular Weight, Density, Chain Dimensions, and Melt Viscoelastic Properties. *Macromolecules* **1994**, *27*, 4639−4647.